C. R. Mecanique 341 (2013) 581–591

Contents lists available at SciVerse ScienceDirect

Comptes Rendus Mecanique

www.sciencedirect.com

Physical based numerical schemes for the discretization of the sediment settling term

Xinhua Lu [a,b,*], Xiaofeng Zhang [a], Bingjiang Dong [c], Huaihan Liu [b], Bing Mao [d]

[a] State Key Laboratory of Water Resources and Hydropower Engineering Science, Wuhan University, Wuhan 430072, China
[b] Changjiang Waterway Planning, Design and Research Institute, Wuhan 430010, China
[c] Yangtze River Scientific Research Institute, Wuhan 430015, China
[d] Hydrology Bureau, Yangtze River Water Resource Commission, Wuhan 430010, China

ARTICLE INFO

Article history:
Received 21 January 2013
Accepted after revision 22 May 2013
Available online 19 June 2013

Keywords:
Sedimentation
Suspension
Mass conservation
Wave breaking
Settling velocity

ABSTRACT

In this paper, the discretization of the sediment settling term is investigated. Two potential problems induced by the incorrect discretization of this term are analyzed. It shows that even the first-order upwind algorithm, the most stable and conservative scheme, cannot always ensure stability and mass conservation. To tackle these issues, three rules are proposed. Based on these rules, two schemes are designed. The performances of different schemes are tested in a study of sediment motions under a wave-breaking situation. The results show that the unphysical problems are relieved or totally avoided by the new schemes.

1. Introduction

The prediction of sediment suspension, transport and interaction processes between flow, sediment, and bed are key problems in river and coastal engineering and has been studied for decades, yet far from having been understood [1,2]. The transport of suspended sediment is governed by the convection–diffusion equation. The only difference between this equation and the conventional convection–diffusion one is that the formal one has a sediment settling term due to the gravitation of the particles.

In previous researches, the SS term has sometimes been neglected for simplicity [3,4]. When the SS term is taken into account, it has either been discretized together with the vertical advection term [5–7], or separately treated as a source term [8,9]. However, to date no attention has been paid to the discretization of this term itself. In fact, as will be shown later in this paper, this term should be carefully treated and casual discretization will cause unphysical predictions. For example, one may notice that the solutions of sediment concentration can fall below zero on some grid points, even if the time step satisfies the Courant number criterion. This is observed by many researchers and usually the concentration is set to zero when the calculated value drops to its lower limit. Suzuki et al. [10] use an alternative method to tackle this problem. When the concentration values in the simulation fall below zero, the numerical fluxes at the control volume interfaces are artificially adjusted so that the total sediment flowing out of the control volume equals the amount of sediment in that cell. Though in this way the concentration is fixed to a physical lower limit, this ad-hoc method affects the correct numerical fluxes at other control volume interfaces and thus mass conservation problem is induced.

In this paper, the potential problems related to the discretization of the SS term are discussed. The physical rules are given to avoid these problems and, based on these rules, two new schemes are proposed. The new schemes and the

* Corresponding author at: State Key Laboratory of Water Resources and Hydropower Engineering Science, Wuhan University, Wuhan 430072, China.
E-mail address: XHLUHH@aliyun.com (X.H. Lu).

1631-0721/$ – see front matter
http://dx.doi.org/10.1016/j.crme.2013.05.002

conventional one are then tested. The results show that our new schemes are superior to the conventional one and that the potential problems caused by the incorrect discretization of the SS term are partly or totally avoided.

2. Numerical model

2.1. Governing equations

The large-eddy simulation (abbreviated as LES hereinafter) governing equations for an air–water two-phase flow can be expressed by:

$$\frac{\partial \boldsymbol{u}}{\partial t} + \nabla \cdot (\boldsymbol{u}\boldsymbol{u}) = -\frac{1}{\rho}\nabla \Pi + \frac{\mu}{\rho}\nabla \cdot (2\overline{D}) - g\boldsymbol{j} - \frac{1}{\rho}\gamma\kappa\delta(\phi)\nabla\phi - \boldsymbol{F} \tag{1}$$

$$\nabla \cdot \boldsymbol{u} = 0 \tag{2}$$

and the governing equation for sediment transport is:

$$\frac{\partial s}{\partial t} + \frac{\partial (u_i - \omega_s \delta_{i2}) s}{\partial x_i} = \frac{\partial}{\partial x_i}\left(\frac{(\nu + \nu_{SGS})}{Sc_t}\frac{\partial s}{\partial x_i}\right) \tag{3}$$

where, $\boldsymbol{u} = (u, v, w)$ is the flow vector and u, v, w are the flow components in streamwise x, vertical y and spanwise z directions, respectively; t denotes time; $\Pi = P_d + P_h$ denotes total pressure and P_h and P_d are respectively hydrostatic and dynamic pressures; $\overline{D}_{ij} = (\partial u_i/\partial x_j + \partial u_j/\partial x_i)/2$ is the deformation tensor; g is the acceleration of gravity and $\boldsymbol{j}$ is the unit vector in the vertical direction; $\boldsymbol{F}$ denotes the subgrid-scale stress terms and $\boldsymbol{F}_i = \frac{\partial \tau_{ij}}{\partial x_j} = \frac{\partial(\overline{u_i u_j} - \overline{u}_i \overline{u}_j)}{\partial x_j}$; $\delta(\phi) = \frac{dH(\phi;\epsilon)}{d\phi}$, here $H(\phi;\epsilon)$ is the Heaviside function; ϕ denotes the level-set distance function, negative in the air and positive in water; γ is surface tension coefficient; ϵ is half width of the air–water interface smoothing thickness; $\kappa = -\nabla \cdot (\frac{\nabla\phi}{|\nabla\phi|})$ denotes the interface curvature; s is the sediment concentration in volume; δ_{ij} is the Kronecker operator; Sc_t is the Schmidt number [6,11]. The density and the dynamic viscosity, ρ and μ, are expressed respectively as:

$$\rho(\phi) = \rho_a + (\rho_w - \rho_a) \cdot H(\phi;\epsilon) \tag{4}$$

$$\mu(\phi) = \mu_a + (\mu_w - \mu_a) \cdot H(\phi;\epsilon) \tag{5}$$

and in this study, a mollified Heaviside function $H(\phi;\epsilon)$ is adopted:

$$H(\phi;\epsilon) = \begin{cases} 1 & \phi > \epsilon \\ \frac{1}{2}\left(1 + \frac{\phi}{\epsilon} + \frac{1}{\pi}\sin\left(\frac{\phi\pi}{\epsilon}\right)\right) & |\phi| \leqslant \epsilon \\ 0 & \phi < -\epsilon \end{cases} \tag{6}$$

In Eq. (3), ω_s is the sediment settling velocity and $\frac{\partial \omega_s s}{\partial y}$ is the SS term discussed in this paper. Due to the low concentration in the simulation, the effect of concentration on sediment settling velocity is neglected and is calculated as [12]:

$$\omega_s = \sqrt{\left(13.95\frac{\nu_w}{d_{50}}\right) + 1.09\frac{\rho_s - \rho_w}{\rho_w} g d_{50}} - 13.95\frac{\nu_w}{d_{50}} \tag{7}$$

where d_{50} is the sediment particle diameter. The subscripts "a," "w," and "s" denote air, water, and sediment, respectively, i.e., ν_w denotes the kinematic viscosity of water.

2.2. Subgrid-scale stress

To account for the unsolved subgrid motions, the widely used RNG-LES model [13,14] is used. This model is based on the renormalization group theory and has no tunable coefficients. Besides, this model can predict rational subgrid-scale stress near the wall.

In the framework of RNG-LES, τ_{ij} is modeled based on the viscosity concept as:

$$\tau_{ij} - \frac{1}{3}\tau_{kk}\delta_{ij} = -2\nu_{SGS}\overline{D}_{ij} \tag{8}$$

and ν_{SGS} is iterated obtained from:

$$\nu_{SGS} + \nu = \nu\left[1 + H\left(\frac{\nu_s^2 \cdot (\nu_{SGS} + \nu)}{\nu^3} - C\right)\right]^{1/3} \tag{9}$$

in which $\nu_s = C_{RNG}\Delta^2\sqrt{2\overline{D}_{ij}\overline{D}_{ij}}$. H is expressed as:

$$H(x) = \begin{cases} x & x > 0 \\ 0 & \text{otherwise} \end{cases} \tag{10}$$

In the above equations, $C = 75$ and $C_{RNG} = 0.0062$ are RNG-LES constants [13].

2.3. Discretization and solution methods

The governing equations for flow, Eqs. (1) and (2), are discretized using a finite difference scheme, and Eq. (3) is discretized using the finite volume method. All the discretization is implemented on a staggered-MAC-type grid [15]. For Eqs. (1) and (2), the central difference scheme is used for spatial discretization. When strong free-surface motion exists (i.e., in a wave-breaking environment), an essentially non-oscillatory scheme is applied to ensure stability. For the sediment transport equation, the HLPA scheme [16] is used to discretize the convection term. As suggested by previous researchers [11,6], the first-order upwind scheme is used for the bottommost five grids to ensure stability where a strong concentration gradient exists.

For the time derivative, a second-order explicit Runge–Kutta scheme is used. The velocity field is made divergence-free by using the projection method [17]. The code is parallelized based on the Message Passing Interface (MPI) method, and the Bi-CGSTAB method [18] is used for the solution of Poisson equation for dynamic pressure.

2.4. Near-bed boundary conditions

As proposed by Chou and Fringer [6,19], the bottom flux of sediment is calculated based on the physical erosion flux E and the deposition flux D, which read respectively as:

$$E(t) = p_{\mathrm{k}}(t) = \begin{cases} 0.00033\left(\frac{\theta(t)-\theta_{\mathrm{c}}}{\theta_{\mathrm{c}}}\right)^{1.5} \frac{(\rho_{\mathrm{s}}/\rho_{\mathrm{w}}-1)^{0.6} g^{0.6} d_{50}^{0.8}}{\nu_{\mathrm{w}}^{0.2}} & \theta(t) > \theta_{\mathrm{c}} \\ 0 & \text{else} \end{cases} \tag{11}$$

$$D(t) = \omega_{\mathrm{s}} s_{\mathrm{bed}} \tag{12}$$

where $p_{\mathrm{k}}(t)$ is the sediment pick-up flux and $\theta(t)$ is the instantaneous Shields parameter calculated by:

$$\theta(t) = \frac{u_*^2}{(\rho_{\mathrm{s}}/\rho_{\mathrm{w}} - 1) g d_{50}} \tag{13}$$

In the above equations, θ_{c} is the critical Shields parameter; u_* is the bottom friction velocity; s_{bed} is the instantaneous sediment concentration at the bed obtained through interpolation from the interior points [6,19,20].

The bottom friction velocity u_* is calculated from [10,21]:

$$u_* = \sqrt{\frac{f_{\mathrm{w}}}{2}} |u_{\mathrm{b}}| \tag{14}$$

In the above equations, u_{b} is the near-bed velocity parallel to the bed; $\kappa = 0.41$ is the von Karman constant and f_{w} is the wave friction coefficient determined by the well-known Nielsen formula [22].

Note that the shear stress calculated above will also provide a boundary condition for the closure of the flow module.

3. Analysis of potential errors in the discretization of the SS term

Seeing that the high-order schemes reduce to stable low-order schemes automatically and that a first-order upwind scheme is suggested, especially in the near-bottom grids, by many investigators [6,11,19,23,24], we analyze the potential errors rose from the SS-term discretization based on the first-order upwind scheme. Two typical problems will be demonstrated and it will be shown that even the most stable and conservative first-order upwind scheme (named as the conventional upwind scheme hereafter) cannot always ensure stability or mass conservation.

3.1. Problem I: Isolated concentration point and the induced mass non-conservation problem

For simplicity, the vertical two-dimensional issue is discussed and the method described here can be directly used in the 3D analyses. Fig. 1 illustrates the typical flow field for this problem. Also shown are the staggered variables.

Let us assume that:

(i) the vertical velocity component around the control volume $s_{i,j}$ is small (say, less than the sediment settling velocity ω_{s});
(ii) initially (or at the last time step), the sediment concentration of $s_{m,j}$ $(m = i-1, i+1)$ is small and for simplicity assumed to be zero;
(iii) the diffusion term in Eq. (3) is omitted;

then the sediment fluxes at the interfaces of the control volume $s_{i,j}$ can be calculated as shown in Table 1. Note that $Flux_{\mathrm{L}}$ and s_{L} correspond to the sediment flux and concentration at the left interface of the control volume $s_{i,j}$ and a similar definition is used for sediment fluxes at other interfaces. The total sediment flux $\sum F_{\mathrm{s}}$ is then obtained by summing up the second column of Table 1. It is easy to obtain that $\sum F_{\mathrm{s}} < 0$. From Eq. (3), we know that the sediment concentration

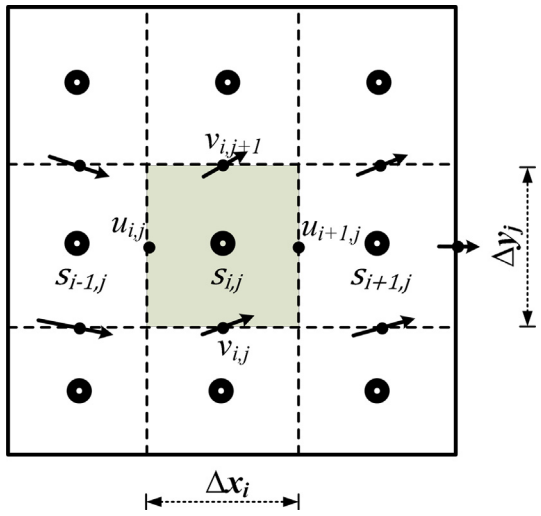

Fig. 1. Sketch of the flow field for Problem I.

Table 1
Sediment fluxes at interfaces of control volume $s_{i,j}$.

Interface location	Numerical fluxes	Comment
Left	$Flux_L = u_{i,j} \cdot s_L = 0$	$s_L = 0$
Right	$Flux_R = u_{i+1,j} \cdot s_R = 0$	$s_R = 0$
Bottom	$Flux_B = v_{i,j} \cdot s_B = (v_{i,j} - \omega_s) \cdot s_{i,j-1} < 0$	$v_{i,j} < \omega_s$
Up	$Flux_T = v_{i,j+1} \cdot s_T = (v_{i,j+1} - \omega_s) \cdot s_{i,j} = 0$	$s_{i,j} = 0$

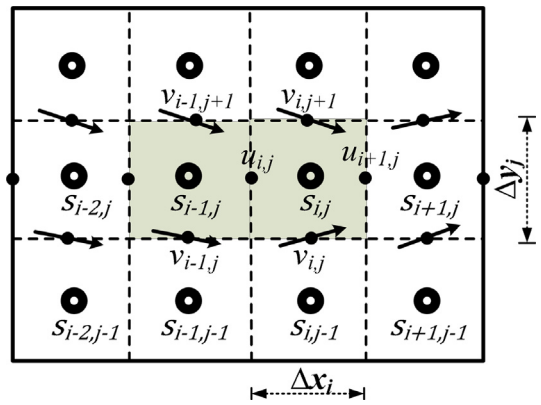

Fig. 2. Sketch of the flow field for Problem II.

will be less than zero at the next time step. As aforementioned, to avoid this unphysical value, a threshold value is usually prescribed and for this situation $s_{i,j} = 0$ is imposed. This treatment contributes to an isolated concentration point at point $s_{i,j}$ and will cause mass non-conservation problems, since the sediment fluxes are not conserved.

3.2. Problem II: Unphysical discontinuous field of sediment concentration

The typical flow field for this problem is shown in Fig. 2.
Similar as in the analysis in Problem I, we assume that:

(i) the vertical velocity component around the control volume $s_{m,j}$ $(m = i-1, i)$ is small (i.e., less than ω_s);
(ii) initially (or at the last time step), the sediment concentration of $s_{m,n}$ $(m = i-2, i+1;\ n = j, j+1)$ is small and for simplicity assumed to be zero; the sediment concentration is positive at the bottom cells $s_{m,j-1}$ $(m = i-2, i+1)$ and has values that cannot be neglected;
(iii) the diffusion term in Eq. (3) is omitted.

The sediment fluxes around the control volume $s_{i-1,j}$ and $s_{i,j}$ can now be calculated. The only fluxes that make sense are at the bottom interfaces since other fluxes are zero. Thus, we have: for control volume $s_{i-1,j}$, the vertical velocity at the bottom is negative and thus the bottom flux is calculated based on the upwind node as:

$$\begin{aligned} Flux_{\mathrm{B}} &= (v_{i-1,j} - \omega_{\mathrm{s}}) \cdot s_{i-1,j} \\ &= (v_{i-1,j} - \omega_{\mathrm{s}}) \cdot 0 = 0 \end{aligned} \tag{15}$$

and for control volume $s_{i,j}$, the vertical velocity at the bottom is positive and thus:

$$\begin{aligned} Flux_{\mathrm{B}} &= (v_{i,j} - \omega_{\mathrm{s}}) \cdot s_{i,j-1} \\ &\approx -\omega_{\mathrm{s}} \cdot s_{i,j-1} \lessapprox 0 \end{aligned} \tag{16}$$

Here $\lessapprox$ means less than but cannot be neglected. The changes of direction in the vertical velocity then cause rather different fluxes at neighboring points $s_{i-1,j}$ and $s_{i,j}$. It is unreasonable. Since a small vertical velocity is assumed, the bottom sediment fluxes should not be significantly different, especially when both $v_{i-1,j}$ and $v_{i,j}$ approach zero. The discontinuous bottom fluxes will finally lead to unphysical discontinuous sediment concentration fields.

It must be stressed that: (a) Problem I can occur everywhere in a simulation domain, while Problem II usually occurs where large sediment gradient and recirculation (direction of vertical velocity changes) exists; (b) the two problems are related to the numerical discretization of the SS term and the problems will not vanish when the SS term is treated as a source term [8,9]; (c) if the Courant number approaches 1, the numerical solution will not be stable for an explicit scheme and may cause an unphysical concentration field—this is not the issue discussed in this study; (d) by using fine grids, the adverse effect caused by the two problems might be reduced, but can hardly be avoided. Point (d) will be revisited further in Section 5.

4. New sediment schemes for the discretization of the SS term

To address the two issues in Section 3 and to design a reasonable numerical scheme for sediment flux in the vertical direction, the following three physical based rules should be satisfied:

(a) when the vertical velocity is negative, due to the negative settling velocity, the conventional upwind scheme should be used to calculate interface concentration and the vertical sediment flux;
(b) when the vertical velocity is positive but has a small value, the conventional upwind scheme may induces the two problems described above;
(c) when the vertical velocity is positive and sufficiently large, the conventional upwind method should have no problem since at this time much information is coming from the bottom cells.

Based on the above rules, two schemes are designed for interface concentration calculations, as follows.

Scheme 1.

$$s_{i,j-\frac{1}{2}} = \begin{cases} s_{i,j} & v_{i,j} < 0 \\ \beta s_{i,j-1} + (1-\beta) s_{i,j} & v_{i,j} \geqslant 0 \end{cases} \tag{17}$$

here, $\beta = \min(v_{i,j}/\omega_{\mathrm{s}}, 1.0)$.

Scheme 2.

$$s_{i,j-\frac{1}{2}} = \begin{cases} s_{i,j-1} & v_{i,j} \geqslant v_{\mathrm{p}} \\ s_{i,j} & v_{i,j} < v_{\mathrm{p}} \end{cases} \tag{18}$$

In Scheme 1, when $v_{i,j}$ is negative, the scheme is designed according to rule (a); when $v_{i,j}$ is positive, the interface value is smoothly constructed by using both upper and bottom cell information; when $v_{i,j}/\omega_{\mathrm{s}} > 1.0$, where a strong vertical velocity exists, information totally comes from the bottom cells (rule (c) satisfied).

Scheme 2 is designed to directly satisfy all the three rules. The form of Eq. (18) is just like a newly defined "upwind" scheme. The difference with the conventional upwind scheme is that the judging condition for vertical velocity is not zero, but v_{p}. Obviously, the threshold value v_{p} should be related to the sediment settling velocity ω_{s}. In this paper, $v_{\mathrm{p}} = \alpha\omega_{\mathrm{s}}$ is assumed.

5. Test of SS schemes in the study of sediment motions under a wave-breaking situation

In a coastal region, the sediment is suspended by the powerful breaking waves and then transported by the breaking-wave-induced mean flow or tidal currents. In this simulation, a vertical 2D periodic wave propagating on a flat seabed

Table 2
Parameters used in the simulation.

h_w (m)	h_a (m)	λ (m)	T (s)	ak	ρ_s (kg/m^3)	ρ_w (kg/m^3)	d_{50} (m)	ω_s (m/s)
0.1	0.24	1.4	1.46	0.25	2650	1000	0.0001	0.006

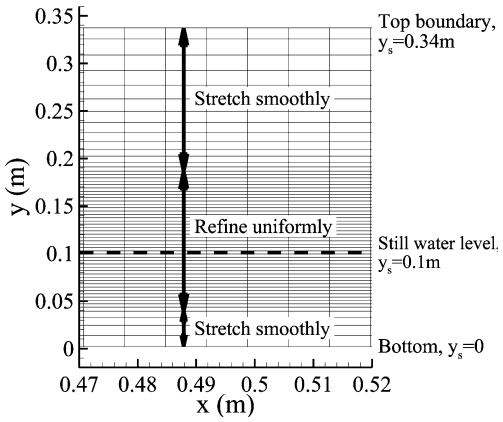

Fig. 3. Grid layout for the simulation (400×180). The grid is shown every 2×3 grid for clear illustration. The dotted line represents the still-water level.

is studied. At the top boundary, a shear-free condition is applied. The bottom boundary for flow and sediment is treated according to the methodology explained in Section 2.4. The bed deformation is omitted as in other works [6,25] due to the rather small time scale.

The depth for water h_w and for air h_a is chosen as 0.1 m and 0.24 m, respectively. Here the large air layer depth is adopted to reduce the lid effect on the top boundary. The wavelength λ and the wave period T are chosen as 1.4 m and 1.46 s, respectively. The initial wave slope ak is set to 0.25. The sediment density ρ_s and the particle diameter d_{50} are set to 2650 kg/m^3 and 0.0001 m according to the practical situations in an oceanic environment. The sediment settling velocity is about 0.006 m/s. The concrete parameters used in the simulation are listed in Table 2.

For air–water interface modeling, the advanced coupled level set (LS) and volume-of-fluid (VOF) method, CLSVOF, is adopted [26,27]. In this method, the spatial gradient in VOF solutions is calculated based on the continuous signed LS distance functions, while the accurate mass conservation property is achieved by using the conservative VOF functions. The initial condition for flow is obtained based on the linear wave theory. As the initial wave slope is high, the wave will not be stable and will break. This method is widely used to generate breaking waves [14,28]. The initial sediment concentration is set to zero. We use fine grids in the simulation (400×180), as shown in Fig. 3. The grid is evenly distributed in the streamwise direction. To resolve the strong air–water interface motions, especially the different scales of air bubbles generated in the wave-breaking process, the grid is refined in the interval $y_s - a < y < y_s + 1.5a$ with a uniform grid width of 0.0005 m. The grid is then stretched to the top and bottom boundary with the largest grid width of 0.0049 m in the top air cells. The time step is 0.00008 s, under which the Courant number is far below 1.

Several instantaneous flows and sediment concentration flow fields are illustrated in Fig. 4. In the pre-breaking stages (Fig. 4(a), (b)), the air–water interface becomes asymmetric and a jet is formed near the wave crest. During this stage, the sediment is picked up by the high shear stress near the bottom. As the wave propagates forward, the interface overturns and touches the downstream surface (Fig. 4(c), (d)). In these stages, the sediment is successively suspended and then transported upward by the vertical velocity. As we focus on the SS-term schemes here, we do not go further into the details of the physical process.

For conventional upwind scheme, Fig. 4(a) shows the unphysical sediment concentration distributions near the bottom. Two discontinuous areas exist around $x = 0.4\lambda$ and $x = 0.6\lambda$, marked as A1 and A2 in Fig. 4(a), respectively. These areas are where the vertical velocity is small (compared to sediment settling velocity) and where changes in the direction of the vertical velocity happen (Problem II occurs). The left discontinuous area disappear around $0.21T$ (Fig. 4(b)), and then, at $t = 0.43T$ (Fig. 4(d)), an isolated concentration area occurs around $x = 0.55\lambda$ (marked as A3 in Fig. 4(d)). The detailed local concentration flow and concentration field around area A3 is shown in Fig. 5. Also shown is the vertical velocity distribution along the x-direction through the isolated concentration point (Fig. 5(b)). We see that the vertical velocity is slightly greater than zero but less than the sediment settling velocity around area A3. Problem I occurs in this high-concentration-gradient area, and thus an unphysical value is predicted.

If we compare Scheme 1 to the conventional upwind scheme, the sediment concentration in area A1 is much smoother and the discontinuous region around area A2 is reduced. Besides, the isolated concentration point around area A3 disappears. If, as we can see, Scheme 1 cannot handle all the unphysical problems, on the contrary, all the unphysical predictions are resolved by Scheme 2, as shown in Fig. 4(i)–(l). The different results between Scheme 1 and Scheme 2 imply that it is of great importance that all the three rules listed in Section 4 should be satisfied.

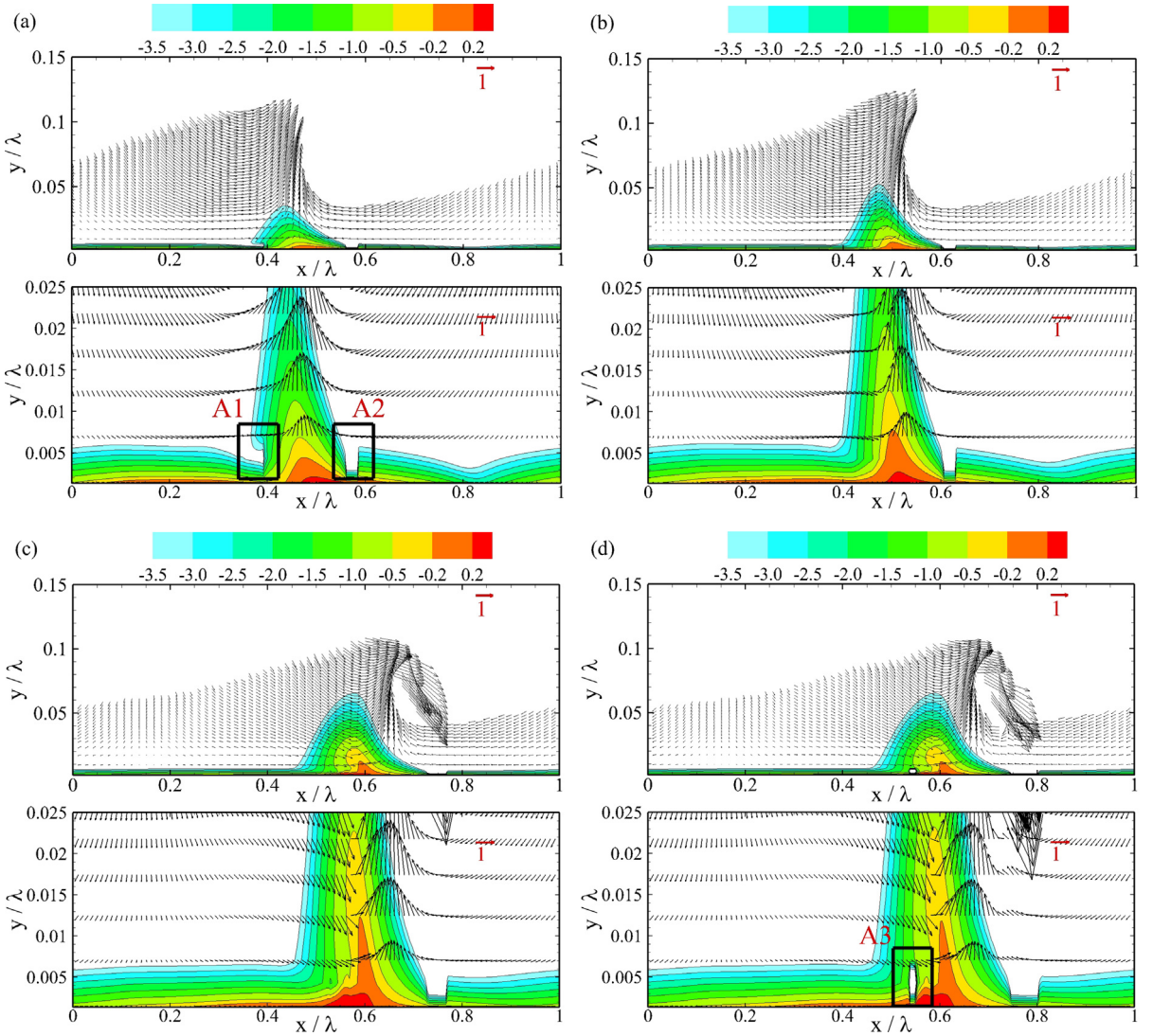

Fig. 4. Instantaneous flow and sediment concentration field (water phase shown only) at $t = 0.21T$, $t = 0.28T$, $t = 0.42T$ and $t = 0.43T$, respectively. (a)–(d) for conventional upwind scheme; (e)–(h) for Scheme 1; (i)–(l) is the result from Scheme 2 with $\alpha = 1.0$. In each subfigure, velocity is shown every 6×3 grid for the upper figure and an enlarged figure (velocity demonstrated every 4×2 grid) is given to show clearly the high-concentration area near the bottom. The sediment concentration is shown by $\log_{10} s$ instead of s for clear illustration. The velocity and concentration is normalized by wave celerity c and s^{av}_{max}, respectively. Here, s^{av}_{max} is the maximum value of s^{av}_b when α equals 1.

To see if the unphysical solutions, i.e., discontinuous areas A1 and A2 in Fig. 4(a), can be avoided by using finer grids, another simulation is carried out with grids doubled in the x-direction. The results are illustrated in Fig. 6. Since the original 400×180-mesh grid is sufficiently fine to resolve the flow structures, the changes in velocity field is negligible when finer grids are used. The comparison of the sediment concentration field shows that the unphysical solutions around areas A1 and A2 are not relieved with finer grids.

The effect of α in Scheme 2 is investigated here. We define a parameter P_{Ai} to show if the unphysical solutions occur in area Ai ($i = 1, 2$). When P_{Ai} equals to unit, unphysical solutions exist in area Ai and the solution is reasonable when P_{Ai} equals zero. The statistics of parameter P_{Ai} is shown in Table 3. Note that for Scheme 2, $\alpha = 0$ is equivalent to the conventional upwind scheme. One can see that when α increases, the unphysical solution is relieved. When $\alpha = 0.4$, the discontinuous area A1 does not exist anymore and the discontinuous area A2 intends to disappear totally when α equals 0.6. Excellent solutions are obtained with α chosen between 0.8 and 1.2. Fig. 7 gives the time history of the averaged near-bed sediment concentration (s^{av}_b) for different values of α. A negligible difference is observed between the results when α varies between 0.8 and 1.2. When α is larger than 1.4, some difference in results occur, which can be clearly seen in the zoom view of Fig. 7. Based on this simulation, optimized values of α in the [0.8–1.2] range are suggested for using in Scheme 2.

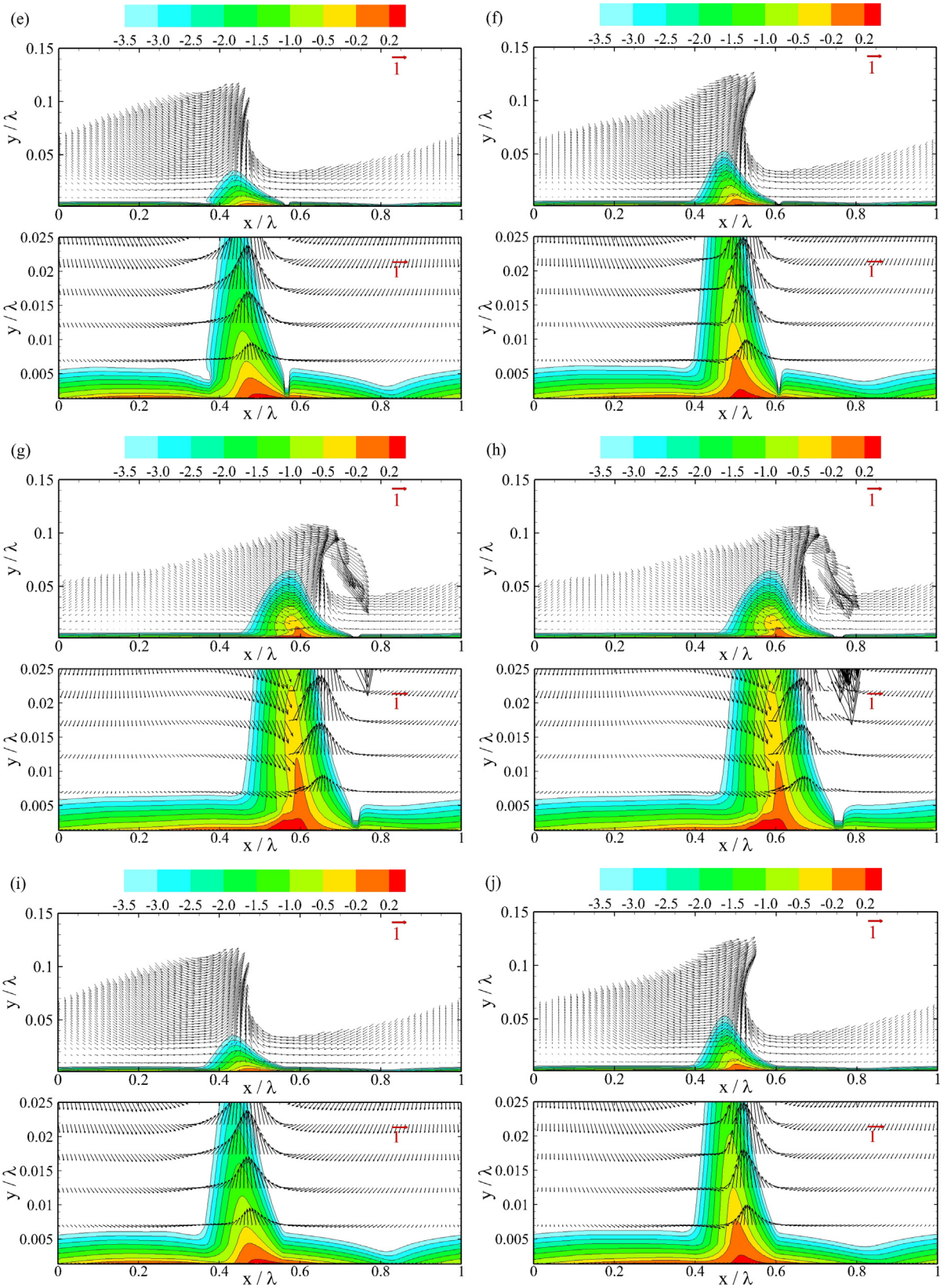

Fig. 4. (*continued*)

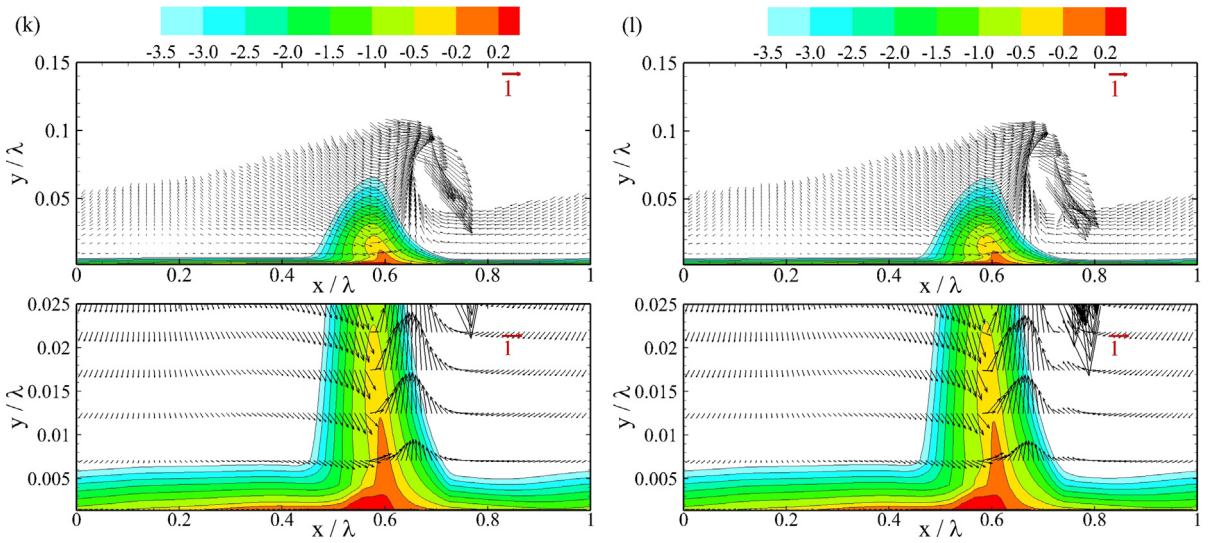

Fig. 4. (*continued*)

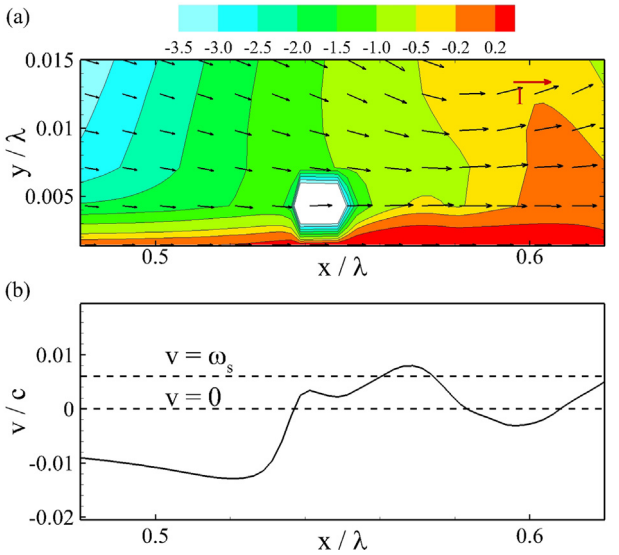

Fig. 5. Local flow field and concentration distribution around area A3 in Fig. 4(d). Velocity vectors are shown every 4×1 grid. Fig. 5(b) gives the vertical velocity distribution along x-direction through the isolated concentration point. In Fig. 5(a), the velocity and concentration is normalized by c and $s_{\max}^{\text{av}}$, respectively.

Table 3
Performance of Scheme 2 with different values of α.

α	P_{A1}	P_{A2}
0.0	1	1
0.2	1	1
0.4	0	1
0.6	0	1
0.8	0	0
1.0	0	0
1.2	0	0

6. Discussion and conclusion

In this paper, a study on the discretization of the sediment settling-related term (SS term) is carried out. The two potential problems are analyzed. The first one is related to the unreasonable mathematical prediction of isolated concentration

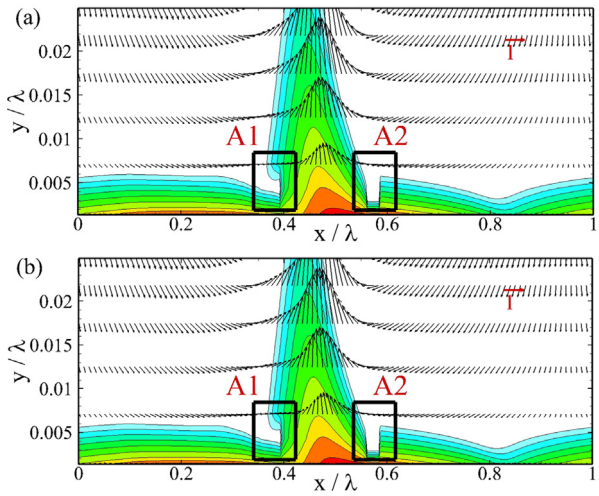

Fig. 6. Instantaneous flow and sediment concentration field (water phase shown only) at $t = 0.21T$ with grid number 400×180 (Fig. 6(a)), and 810×180 (Fig. 6(b)), respectively. The results are obtained from the conventional upwind scheme. The velocity is shown every 4×2 grid in (a) and 8×2 grid in (b) for clear illustration. The sediment concentration is shown using logarithmic scale. The velocity and concentration is normalized by c and $s_{\max}^{\mathrm{av}}$, respectively.

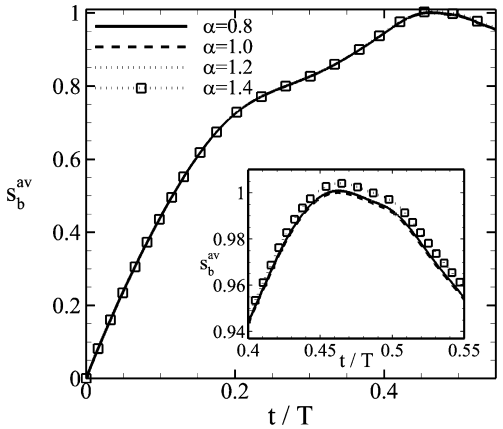

Fig. 7. Time history of near-bed averaged concentration with different values of α for Scheme 2. Results are normalized by $s_{\max}^{\mathrm{av}}$. A zoom view is given in the bottom-right corner to show the differences in time interval between $0.4T$ and $0.55T$.

points which causes mass non-conservation problems. The second one is the unphysical discontinuous sediment concentration field problem that occurs where large sediment gradient and recirculation exist. To satisfy the three rules listed in this paper, two new schemes are proposed. The schemes are then tested in a study of sediment motions under a wave-breaking environment. The two unphysical problems occur when the conventional upwind scheme is used. With Scheme 1, the problems are relieved. The problems totally disappear when Scheme 2 is used. Therefore Scheme 2 is suggested using in vertical 2D and 3D sediment simulations. A sensitivity study on coefficient α (in Scheme 2) is also implemented and a value of α between 0.8 and 1.2 is suggested.

Acknowledgements

This study is part of the research project sponsored by the Fundamental Research Funds for the Central Universities (Grant No. 20102060101000064) and by the National Natural Science Foundation of China (Grant No. 51079104). The first author thanks Dr. X. Guo, Professor L. Shen, and Professor R.A. Dalrymple for discussions in the frame of this study.

References

[1] É. Guazzelli, Sedimentation of small particles: how can such a simple problem be so difficult?, C. R. Mecanique 334 (2006) 539–544.
[2] D. Gonzalez-Rodriguez, O.S. Madsen, Boundary-layer hydrodynamics and bedload sediment transport in oscillating water tunnels, J. Fluid Mech. 667 (2010) 4–84.
[3] C.M. Fang, Q.W. Han, M.M. He, Analysis on plunging conditions of density stratified flow and 2-D simulation, J. Sediment. Res. 4 (1997) 68–75 (in Chinese).
[4] Y. Peng, Y.T. Li, W.X. Huai, 2D vertical numerical solution to the density current plunge flow, J. Sediment. Res. 6 (2000) 25–30 (in Chinese).

[5] H.W. Fang, W. Rodi, Three-dimensional calculations of flow and suspended sediment transport in the neighborhood of the dam for the Three Gorges Project (TGP) reservoir in the Yangtze River, J. Hydraul. Res. 41 (4) (2003) 379–394.
[6] Y.J. Chou, O.B. Fringer, Modeling dilute sediment suspension using large-eddy simulation with a dynamic mixed model, Phys. Fluids 20 (2008) 115103, 13 pp.
[7] C.E. Ozdemir, T.J. Hsu, S. Balachandar, Simulation of fine sediment transport in oscillatory boundary layer, J. Hydro-Environ. Res. 3 (4) (2010) 247–259.
[8] B.C. Liang, H.J. Li, D.Y. Lee, Numerical study of three-dimensional suspended sediment transport in waves and currents, Ocean Eng. 34 (11) (2007) 1569–1583.
[9] J.C. Warner, C.R. Sherwood, R.P. Signell, et al., Development of a three-dimensional, regional, coupled wave, current, and sediment-transport model, Comput. Geosci. 34 (2008) 1284–1306.
[10] T. Suzuki, A. Okayasu, T. Shibayama, A numerical study of intermittent sediment concentration under breaking waves in the surf zone, Coastal Eng. 54 (5) (2007) 433–444.
[11] E.A. Zedler, R.L. Street, Sediment transport over ripples in oscillatory flow, J. Hydraul. Eng. 132 (2) (2006) 180–193.
[12] R. Zhang, J. Xie, Sedimentation Research in China: Systematic Selections, China Water and Power Press, Beijing, 1993.
[13] V. Yakhot, S.A. Orszag, Renormalization group analysis of turbulence I. Basic theory, J. Sci. Comput. 1 (1) (1986) 3–51.
[14] Y. Hu, G. Xin, X.H. Lu, R.R. Dalrymple, L. Shen, Idealized numerical simulation of breaking water wave propagating over a viscous mud layer, Phys. Fluids 24 (2012) 112104, 20 pp.
[15] F.H. Harlow, J.E. Welch, Numerical calculation of time-dependent viscous incompressible flow of fluid with free surface, Phys. Fluids 8 (1965) 2182–2189.
[16] J. Zhu, A low-diffusive and oscillation-free convection scheme, Commun. Appl. Numer. Methods 7 (1991) 225–232.
[17] J. Kim, P. Moin, Application of a fractional-step method to incompressible Navier–Stokes equations, J. Comput. Phys. 323 (1985) 308–323.
[18] H.A. van de Vorst, Bi-CGSTAB: A fast and smoothly converging variant of Bi-CG for the solution of nonsymmetric linear systems, SIAM J. Sci. Comput. 13 (2) (1992) 631–644.
[19] Y.J. Chou, O.B. Fringer, A model for the simulation of coupled flow-bed form evolution in turbulent flows, J. Geophys. Res. 115 (C10041) (2010) 1–20.
[20] L. Amoudry, T.J. Hsu, P.L.F. Liu, Schmidt number and near-bed boundary condition effects on a two-phase dilute sediment transport model, J. Geophys. Res. 110 (C09003) (2005) 1–12.
[21] X. Yu, T.J. Hsu, D.M. Hanes, Sediment transport under wave groups: Relative importance between nonlinear waveshape and nonlinear boundary layer streaming, J. Geophys. Res. 115 (C02013) (2010) 1–18.
[22] P. Nielsen, Coastal Bottom Boundary Layers and Sediment Transport, World Scientific, Singapore, 1992.
[23] H. Kim, Temporal variation of suspended sediment concentration for waves over ripples, Int. J. Sediment. Res. 18 (3) (2003) 248–265.
[24] E.A. Zedler, R.L. Street, Large-eddy simulation of sediment transport: currents over ripples, J. Hydraul. Eng. 127 (6) (2001) 444–452.
[25] Y.C. Bai, C.O. Ng, Large eddy simulation for plunge breaker and sediment suspension, China Ocean Eng. 16 (2) (2002) 151–164.
[26] M. Sussman, E.G. Puckett, A coupled level set and volume-of-fluid method for computing 3D and axisymmetric incompressible two-phase flows, J. Comput. Phys. 162 (2000) 301–337.
[27] D.L. Sun, W.Q. Tao, A coupled volume-of-fluid and level set (VOSET) method for computing incompressible two-phase flows, Int. J. Heat Mass Transfer 53 (4) (2010) 645–655.
[28] P. Lubin, S. Vincent, S. Abadie, J.P. Caltagirone, Three-dimensional large eddy simulation of air entrainment under plunging breaking waves, Coastal Eng. 53 (2006) 631–655.